704 *Inorg. Chem.* **2010**, *49*, 704–713
DOI: 10.1021/ic902006v

Inorganic Chemistry
Article

Formation of $\{[HIPTN_3N]Mo(III)H\}^-$ by Heterolytic Cleavage of H_2 as Established by EPR and ENDOR Spectroscopy

R. Adam Kinney,[†] Dennis G. H. Hetterscheid,[‡] Brian S. Hanna,[‡] Richard R. Schrock,*[,‡] and Brian M. Hoffman*[,†]

[†]*Department of Chemistry, Northwestern University, 2145 Sheridan Road, Evanston, Illinois 60208 and*
[‡]*Department of Chemistry, Massachusetts Institute of Technology, Cambridge, Massachusetts 02139*

Received October 9, 2009

MoN_2 (**Mo** = $[(HIPTNCH_2CH_2)_3N]Mo$, where HIPT = 3,5-(2,4,6-*i*-$Pr_3C_6H_2)_2C_6H_3$) is the first stage in the reduction of N_2 to NH_3 by **Mo**. Its reaction with dihydrogen in fluid solution yields "**Mo**H_2", a molybdenum−dihydrogen compound. In this report, we describe a comprehensive electron paramagnetic resonance (EPR) and $^{1/2}H/^{14}N$ electron nuclear double resonance (ENDOR) study of the product of the reaction between **Mo**N_2 and H_2 that is trapped in frozen solution, **1**. EPR spectra of **1** show that it has a near-axial **g** tensor, **g** = [2.086, 1.961, 1.947], with dramatically reduced **g** anisotropy relative to **Mo**N_2. Analysis of the **g** values reveal that this anion has the Mo(III), $[d_{xz}, d_{yz}]^3$ orbital configuration, as proposed for the parent **Mo**N_2 complex, and that it undergoes a strong pseudo-Jahn−Teller (PJT) distortion. Simulations of the 2D 35 GHz ^1H ENDOR pattern comprised of spectra taken at multiple fields across the EPR envelope (2 K) show that **1** is the $[$**Mo**$H]^-$ anion. The 35 GHz Mims pulsed ^2H ENDOR spectra of **1** prepared with $^2H_2$ show the corresponding $^2H^-$ signal, with a substantial deuterium isotope effect in a_{iso}. Radiolytic reduction of a structural analogue, **Mo**(IV)H, at 77 K, confirms the assignment of **1**. Analysis of the 2D ^{14}N ENDOR pattern for the ligand amine nitrogen further reveals the presence of a linear N_{ax}−Mo−H^- molecular axis that is parallel to the unique magnetic direction (g_1). The ENDOR pattern of the three equatorial nitrogens is well-reproduced by a model in which the Mo−N_{eq} plane has undergone a static, not dynamic, PJT distortion, leading to a range of hyperfine couplings for the three N_{eq}'s. The finding of a nearly axial hyperfine coupling tensor for the terminal hydride bound **Mo** supports the earlier proposal that the two exchangeable hydrogenic species bound to the FeMo cofactor of the nitrogense turnover intermediate, which has accumulated four electrons/protons (E_4), are hydrides that bridge two metal ions, not terminal hydrides.

Introduction

In nature, dinitrogen is reduced to ammonia by nitrogenase enzymes, the most studied and best known being the FeMo nitrogenase.[1−7] The reaction proceeds according to the stoichiometry

$$N_2 + 8e^- + 8H^+ + 16MgATP \rightarrow 2NH_3 + H_2 + 16MgADP + 16P_i$$

A curious feature of this process is the apparently obligatory formation of a mole of dihydrogen per equivalent of dinitrogen reduced,[8] corresponding to a 75% yield of ammonia in terms of reducing equivalents employed. Under ambient conditions, more than 1 equiv of H_2 is formed and yields of ammonia vary between 40 and 60%.[9−11] How dihydrogen is formed and the extent to which its formation is coupled to the reduction of dinitrogen is still unknown. What is known with certainty is that dihydrogen inhibits dinitrogen reduction.[9−11]

In 2003, it was shown that dinitrogen could be reduced catalytically to ammonia with protons and electrons by molybdenum complexes that contain the $[HIPTN_3N]^{3-}$ ligand ($[HIPTN_3N]^{3-} = [(HIPTNCH_2CH_2)_3N]^{3-}$, where HIPT is 3,5-(2,4,6-*i*-$Pr_3C_6H_2)_2C_6H_3$), examples being $[HIPTN_3N]$-MoN_2, $[HIPTN_3N]$Mo−N=NH, and $[HIPTN_3N]MoNH_3$.[12] In the $[HIPTN_3N]$Mo (**Mo**) system, dinitrogen binds end-on to a single Mo and is reduced by repeated alternating additions of a proton and an electron in the manner first

*To whom correspondence should be addressed. E-mail: bmh@northwestern.edu (B.M.H.).

(1) Burgess, B. K.; Lowe, D. L. *Chem. Rev.* **1996**, *96*, 2983−3011.
(2) Eady, R. R. *Chem. Rev.* (*Washington, DC, U.S.*) **1996**, *96* (7), 3013−3030.
(3) Howard, J. B.; Rees, D. C. *Chem. Rev.* **1996**, *96*, 2965−2982.
(4) Dos Santos, P. C.; Igarashi, R. Y.; Lee, H.-I.; Hoffman, B. M.; Seefeldt, L. C.; Dean, D. R. *Acc. Chem. Res.* **2005**, *38* (3), 208−214.
(5) Hardy, R. W. F.; Bottomley, F.; Burns, R. C. *Treatise on Dinitrogen Fixation*; Wiley-Interscience: New York, 1979.
(6) Veeger, C.; Newton, W. E. *Advances in Nitrogen Fixation Research*; Dr. W. Junk/Martinus Nijhoff: Boston, MA, 1984.
(7) Coughlan, M. P. *Molybdenum and Molybdenum-containing Enzymes*; Pergamon: New York, 1980.
(8) Simpson, F. B.; Burris, R. H. *Science* (*Washington, DC, U. S.*) **1984**, *224*, 1095−1097.
(9) Wherland, S.; Burgess, B. K.; Stiefel, E. I.; Newton, W. E. *Biochemistry* **1981**, *20* (18), 5132−40.
(10) Burgess, B. K.; Wherland, S.; Newton, W. E.; Stiefel, E. I. *Biochemistry* **1981**, *20* (18), 5140−6.
(11) Fisher, K.; Dilworth, M. J.; Newton, W. E. *Biochemistry* **2000**, *39* (50), 15570−15577.
(12) Yandulov, D. V.; Schrock, R. R. *Science* (*Washington, DC, U. S.*) **2003**, *301* (5629), 76−78.

Published on Web 12/15/2009

proposed by Chatt et al.[13] Ammonia is formed selectively (no hydrazine is detected) with an efficiency of 55−65% in electrons. The remaining reducing equivalents are used to form dihydrogen. The amount of dinitrogen that can be reduced is limited to ~4 equiv under the conditions employed, in large part (it is believed) because the $[HIPTN_3N]^{3-}$ ligand is removed from the metal in the presence of protons and reducing agent.

Because dihydrogen is formed along with ammonia, both by the **Mo** catalyst and by the nitrogenase enzyme, the dihydrogen chemistry of **Mo**N_2 is of obvious interest. We recently reported[14] that treatment of **Mo**N_2 with H_2 gas generates "**Mo**H_2", which is possibly an actual H_2 complex or possibly the Mo(V) product of the oxidative addition of H_2 to the Mo(III) complex formed by a loss of N_2. We further postulated that rapid H/D scrambling observed in mixtures of H_2, D_2, and **Mo**H_2 occurs because "**Mo**H_2" is in equilibrium with a complex formed by the heterolytic cleavage of H_2, presumed to be a hydrido-Mo(III) with the proton bound to one of the amides. This complex in turn was thought to be in equilibrium with an "arm-off" complex that may be unstable to a loss of the tris-amidoamine ligand.

As a complement to these solution studies, we have carried out a comprehensive electron paramagnetic resonance (EPR) and $^{1/2}H/^{14}N$ electron nuclear double resonance (ENDOR) study of the product of the reaction between **Mo**N_2 and H_2 that is trapped in frozen solution, **1**. This species is particularly relevant as a biomimetic complex in that it is paramagnetic and binds an H_2-derived species. Its characterization thus provides constraints in the analysis of the four-electron reduced (E_4) state of the molybdenum−iron (MoFe) protein of nitrogenase,[15] whose active-site molybdenum−iron cofactor (FeMo-co) has been shown to contain two chemically identical, symmetry-related hydrogenic species with large isotropic hyperfine couplings.[16] The ENDOR measurements of **1** reveal that it is the anionic, hydrido-Mo(III) product of heterolytic cleavage of H_2 (Scheme 1); we discuss its EPR spectrum in terms of the Jahn−Teller effect (JTE) expected for a low-spin Mo(III) in a trigonal environment.

Materials and Methods

Sample Preparation. The **Mo**N_2 complex in solution was converted to **Mo**(III)H_2 by treatment with H_2 gas, as described;[14] solutions of **Mo**(III)H_2 were also prepared by treating solid **Mo**N_2 with H_2 gas, as described,[14] then dissolving in the desired solvent. Upon freezing, the two types of solution gave identical EPR spectra. Solutions of **Mo**(IV)H were prepared as described,[17] then frozen in liquid nitrogen for cryoreduction and subsequent EPR/ENDOR measurements. The **Mo**(IV)H solutions were cryoreduced at 77 K to form [**Mo**(III)H]$^-$ by γ-irradiation.[18]

Scheme 1

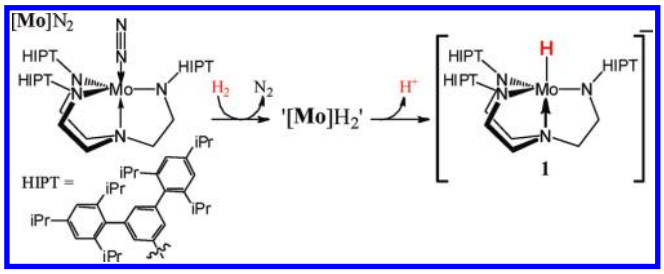

EPR and ENDOR Spectroscopy. X-band EPR was obtained on a modified Bruker ER200 series CW spectrometer with an Oxford Instruments ESR 910 continuous He flow cryostat. Spin quantitations involved double integrations and comparison to a $CuSO_4$ standard (10.2 mM $CuSO_4$, 0.1 M NaCl, and 10 mM EDTA in 80:20 (v/v) water/glycerol) by standard methods.[19] The concentration of **1** was determined by measuring the total concentration of $S = 1/2$ centers at 4 K, then subtracting the concentration of impurity $S = 1/2$ centers as measured at 77 K, a temperature at which the EPR response from **1** is negligible.

The 35 GHz pulsed and CW EPR and ENDOR spectra were obtained at ~2 K on locally constructed instruments described in detail previously.[20−22] The CW measurements employed 100 kHz field modulation and dispersion mode detection under rapid passage conditions. ENDOR spectra employed broadening of the RF to 100 kHz to improve signal-to-noise.[23] Pulsed ENDOR spectra were collected with both Mims and Davies microwave pulse sequences: $\pi/2 - \tau - \pi/2 - T - \pi/2 - \tau - echo$ and $\pi - T - \pi/2 - \tau - \pi - \tau - echo$, respectively, where T is the time interval during which the RF pulse is applied.[24] Data acquisition for all pulse experiments utilized the SpecMan software package[25] (http://specman.4epr.com) in conjunction with a SpinCore PulseBlaster ESR_PRO 400 MHz word generator and an Agilent Technologies Acquiris DP235 500 MS/sec digitizer.

For a single molecular orientation and for nuclei with a nuclear spin of $I = {}^1/_2$ (^{1}H), the ENDOR transitions for the $m_s = \pm{}^1/_2$ electron manifolds are observed at frequencies dictated by the equation

$$\nu_\pm = |\nu_n \pm A/2|$$

where ν_n is the nuclear Larmor frequency and A is the orientation-dependent hyperfine coupling. For $I \geq 1$ (^{2}H, ^{14}N), the two ENDOR lines are further split by the orientation-dependent nuclear quadrupole interaction ($3P$). The peaks are then observed at frequencies dictated by a modified version of the equation above:

$$\nu_{\pm,\pm} = |\nu_\pm \pm 3P/2|$$

In the Mims experiment, the ENDOR intensities are modulated by the response factor inherent to the experiment, which is a function of the product $A\tau$, and given by the equation

$$R \sim [1 - \cos(2\pi A\tau)]$$

(13) Chatt, J.; Dilworth, J. R.; Richards, R. L. *Chem. Rev.* **1978**, *78*, 589−625.
(14) Hetterscheid, D. G. H.; Hanna, B. S.; Schrock, R. R. *Inorg. Chem.* **2009**, *48* (17), 8569−8577.
(15) Lukoyanov, D.; Pelmenschikov, V.; Maeser, N.; Laryukhin, M.; Yang, T. C.; Noodleman, L.; Dean, D.; Case, D.; Seefeldt, L.; Hoffman, B. *Inorg. Chem.* **2007**, *46* (26), 11437−11449.
(16) Igarashi, R. Y.; Laryukhin, M.; Santos, P. C. D.; Lee, H.-I.; Dean, D. R.; Seefeldt, L. C.; Hoffman, B. M. *J. Am. Chem. Soc.* **2005**, *127* (17), 6231−6241.
(17) Yandulov, D. V.; Schrock, R. R.; Rheingold, A. L.; Ceccarelli, C.; Davis, W. M. *Inorg. Chem.* **2003**, *42* (3), 796−813.
(18) Davydov, R.; Makris, T. M.; Kofman, V.; Werst, D. W.; Sligar, S. G.; Hoffman, B. M. *J. Am. Chem. Soc.* **2001**, *123*, 1403−1415.
(19) Pilbrow, J. R. *Transition Ion Electron Paramagnetic Resonance*; Clarendon Press: Oxford, 1990.
(20) Werst, M. M.; Davoust, C. E.; Hoffman, B. M. *J. Am. Chem. Soc.* **1991**, *113* (5), 1533−1538.
(21) Davoust, C. E.; Doan, P. E.; Hoffman, B. M. *J. Magn. Reson.* **1996**, *119*, 38−44.
(22) Zipse, H.; Artin, E.; Wnuk, S.; Lohman, G. J. S.; Martino, D.; Griffin, R. G.; Kacprzak, S.; Kaupp, M.; Hoffman, B.; Bennati, M.; Stubbe, J.; Lees, N. *J. Am. Chem. Soc.* **2009**, *131*, 200−211.
(23) Hoffman, B. M.; DeRose, V. J.; Ong, J. L.; Davoust, C. E. *J. Magn. Reson.* **1994**, *110*, 52−57.
(24) Schweiger, A.; Jeschke, G. *Principles of Pulse Electron Paramagnetic Resonance*; Oxford University Press: Oxford, U. K., 2001; p 578.
(25) Epel, B.; Gromov, I.; Stoll, S.; Schweiger, A.; Goldfarb, D. *Concepts Magn. Reson., Part B* **2005**, *26B* (1), 36−45.

When $A\tau = n$ ($n = 0, 1, 2, ...$), the ENDOR response is at a minimum, resulting in hyperfine "suppression holes" in Mims spectra.

At the low and high field edges of the EPR spectrum (g_1 and g_3, respectively), ENDOR interrogates only a single molecular orientation ("single-crystal-like" position). At intermediate fields, however, ENDOR interrogates a well-defined subset of molecular orientations. By analyzing a 2D field-frequency ("orientation-selective") pattern of ENDOR spectra taken at numerous fields across the EPR envelope, it is generally possible to elucidate the complete hyperfine and quadrupole tensor principal values and their orientations relative to **g**.[26,27]

Hyperfine Sign Determination. Signs of the hyperfine couplings measured from ENDOR spectra (more specifically, the sign of $g_{Nuc}A_{Nuc}$) were obtained by the Pulse-Endor-SaTuration-REcovery (PESTRE) protocol,[28] a pulse sequence comprised of multiple Davies ENDOR sequences, carried out in three distinct experimental phases: (I) an EPR saturation phase (RF off) of 100 Davies sequences whose spin−echo intensities quickly converge to the steady-state "baseline" (BSL); (II) an ENDOR perturbation phase of 24 sequences, in which each sequence contains a fixed RF set at one or the other of the branches of the ENDOR spectrum; and (III) an EPR recovery phase (RF off) of 388 sequences during which the spin echo corresponds to the spin−echo "dynamic reference level" (drl) associated with ENDOR-induced spin polarization created in the second phase, with the drl relaxing to the BSL during this phase. In the slow-relaxation regime, the sign of A_{Nuc} is unambiguously given by the sign of the difference between the drl and BSL echo intensities as observed for *either* ENDOR branch. The exact time-dependent solution[28] of the master equation[29,30] for the electron/nuclear spin populations after each Davies pulse sequence in a multipulse sequence shows that when $A_{Nuc} > 0$ (and $g_{Nuc} > 0$): if ν_+ is being interrogated, the drl relaxes to the BSL from *below*; when ν_- is being interrogated, the drl relaxes to the BSL from *above*. When $A_{Nuc} < 0$, the opposite behavior is observed.

Results

EPR Measurements of 1. Figure 1 shows a reference X-band EPR spectrum of **Mo**N_2 in a frozen toluene solution at 4 K. It has an axial, strongly anisotropic **g** tensor, $g_{\|} = 3.03 > g_e > g_{\perp} = 1.61$, that is associated with the Jahn−Teller (JT) distortion of the low-spin ($S = 1/2$) orbitally degenerate Mo(III) ion in an [e^3] orbital configuration.[31] Upon freezing a solution of **Mo**H_2 in toluene or a 1:9 2-Me THF/THF solution, prepared by either method described above, the **Mo**N_2 signal is found to have disappeared and been replaced by that of the trapped product (**1**) of reaction between **Mo**N_2 and H_2 (Figure 1). This spectrum again is almost axial, with $g_1 > g_e > g_2 \sim g_3$, but with the components of **g** far closer to the free-electron **g** value: **g** = [2.086(18), 1.961(11), 1.947(8)].

Quantitation of the EPR signal of **1** relative to a $CuSO_4$ standard shows that the conversion from **Mo**N_2 to **1** is far from quantitative, typically under half, with most of the parent **Mo**N_2 complex being converted to an unidentified, EPR-silent material; in addition, a relatively weak, unassigned $S = 1/2$ signal can be seen superimposed on the majority signal (Figure 1, inset). Frozen-solution spectra of **1** in different solvents differ minimally, unlike the case for **Mo**N_2. As a frozen solution of **1** is warmed above 4 K, its signal broadens and weakens, disappearing by 70 K and leaving the weak impurity signal. During this process, the g_1 of **1** decreases slightly, from 2.090 to 2.085. For reasons to be discussed below, solutions of **1** in 1:9 2-Me THF/THF were saturated with the salts [Bu_4N][BAr_F] or Na[BAr_F]. This caused only small changes to the principal **g** values, ~0.001−0.003.

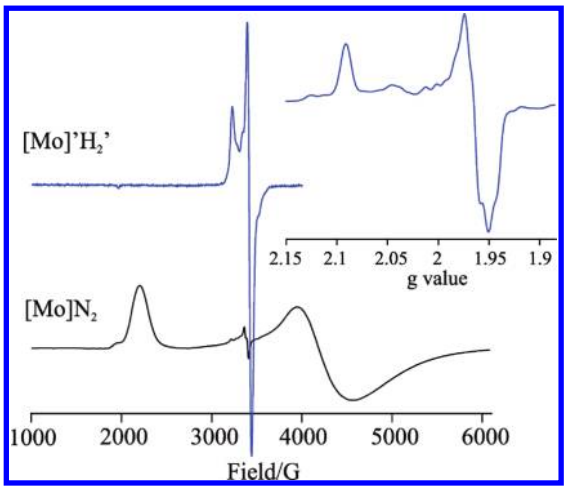

Figure 1. Comparison between 4 K X-band CW EPR of **Mo**N_2 (black), $g_{\|} = 3.03$ and $g_{\perp} = 1.6$, and **1** (blue), **g** = [2.086, 1.961, 1.947], both in frozen toluene solution. Inset: Expanded view of the spectra of **1** in frozen toluene solution. Conditions: Microwave frequency, 9.365 GHz; modulation amplitude, 2.8 G; microwave power, 0.632 mW; temperature, 11 K; scan time, 120 s; time constant, 80 ms.

The **g** values of **1** are consistent with its assignment as a Mo(III) metal center, in that the unique **g** value (g_1) is greater than the free-electron **g** value, rather than less, as would be expected for a Mo(V) center. With a near-axial **g** tensor, the unique **g** value (g_1) is expected to lie roughly parallel to the idealized 3-fold molecular symmetry, thus coinciding with the Mo−N_{ax} bond of the **Mo** system and perpendicular to the plane defined by the Mo−N_{amido} bonds of the $HIPTN_3N^{3-}$ ligand.

It is useful to discuss the **g** values of **1** in terms of the influence of a linear JT distortion on the Mo(III) [e^3] configuration, following the treatment presented for [**Mo**]N_2.[31] This incorporates linear vibronic coupling of the d electrons into a single composite ("interaction") e_2 mode (effective force-constant K, and effective coupling parameter F), which competes with the spin−orbit coupling (SOC) and results in a "pseudo Jahn−Teller effect", PJTE. A distortion, ρ, along the interaction coordinate mixes the e_1 orbitals and lowers the vibronic energy relative to the symmetric structure. Ignoring SOC to the other d orbitals, the **g** values are determined by r, the ratio of the off-diagonal matrix element that generates the splitting of the degenerate [e] = [d_{xz}, d_{yz}] orbitals, V_δ, to the SOC parameter, λ, eq 1; V_δ is equal to the sum of the equilibrium JT distortion energy, V_{JT}, plus a possible "environmental energy", V_E. For example, in the case of **Mo**N_2, V_E is associated with solvent interactions, denoted

(26) Hoffman, B. M. *Acc. Chem. Res.* **1991**, *24*, 164−170.
(27) Doan, P. E. The Past, Present, and Future of Orientation-Selected ENDOR Analysis: Solving the Challenges of Dipolar-Coupled Nuclei. In *Paramagnetic Resonance of Metallobiomolecules*; Telser, J., Ed.; American Chemical Society: Washington, DC, 2003; pp 55−81.
(28) Doan, P. E., *J. Magn. Reson.*, submitted.
(29) Epel, B.; Poppl, A.; Manikandan, P.; Vega, S.; Goldfarb, D. *J. Magn. Reson.* **2001**, *148* (2), 388−397.
(30) Yang, T.-C.; Hoffman, B. M. *J. Magn. Reson.* **2006**, *181*, 280−286.
(31) McNaughton, R. L.; Chin, J. M.; Weare, W. W.; Schrock, R. R.; Hoffman, B. M. *J. Am. Chem. Soc.* **2007**, *129* (12), 3480−3481.

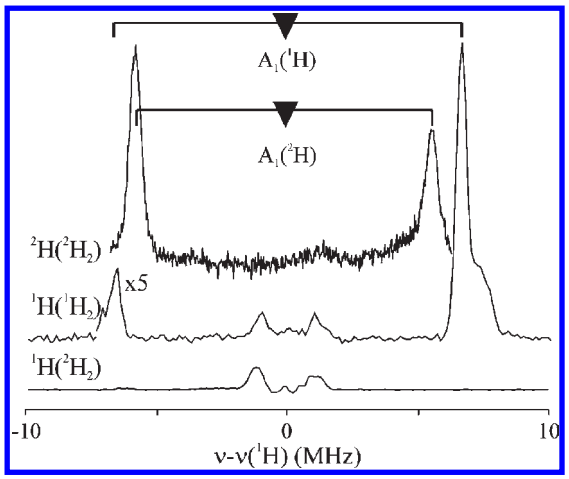

Figure 2. ^{1}H stochastic CW field-modulated ENDOR and ^{2}H Mims ENDOR spectra of **1** and **1(D)** at g_1. The frequency axis of the ^{1}H spectrum has been scaled by the ratio of the nuclear g values ($g_n(^1H)/g_n(^2H) = 6.51$), thus allowing it to be plotted on the ^{1}H frequency axis. Conditions, ^{1}H stochastic CW: microwave frequency, 35.273−35.305 GHz; modulation amplitude, 0.66 G; microwave power, 0.1 mW; temperature, 2 K stochastic sequence (delay/sample/RF), 0.75/1.25/0.5 ms; the RF excitation was broadened to 50 kHz. Conditions, ^{2}H Mims: microwave frequency, 34.914−34.967 GHz; $\pi/2 = 50$ ns; $\tau = 500$ ns; repetition time, 20 ms; RF pulse length, 30 μs; 1 shot per RF point; the RF was randomly hopped.

by V_L. The ratio r is conveniently used to define a fictitious angle, 2θ:

$$r \equiv \tan 2\theta \equiv 2V_\delta/\lambda \equiv 2[V_{JT} + V_E/2]/\lambda \qquad (1)$$

allowing the **g** values to be written in terms of 2θ:

$$g_{\|} = 2(1 + cos\ 2\theta) \qquad (2a)$$

$$g_{\perp} = (2\ sin\ 2\theta) \qquad (2b)$$

As r increases, 2θ increases from 0 (JTE quenched; no distortion) to $\pi/2$ (strong splitting of e_1 degeneracy; real e_1 orbitals), and the **g** values traverse the range, $[4 \geq g_{\|} \geq 2 \geq g_{\perp} \geq 0]$. For comparison, $g_{\|} \sim 3$ for [**Mo**]L, L = N_2/CO, corresponds to $r \sim 1$, whereas $g_{\|} \approx 2.09$ for **1** corresponds to $r \sim 20$. Thus, although the **g** shifts are much smaller than for **Mo**N_2, the **g** tensor for **1** is compatible with an [e^3] orbital configuration, but with a much larger splitting of the e-orbital degeneracy than that experienced by **Mo**N_2. Indeed, the extent of the splitting of the d_π orbitals is so great that one could alternatively treat the value for $g_{\|}$ in terms of an electron in a single, real, d_π orbital coupled by SOC to the other d_π orbital, to second order.[19] However, the Discussion, below, makes it clear why the PJT perspective is useful. In either case, the slight splitting of g_2 and g_3 for **1** is attributable to the influence of second-order contributions to **g** from other d orbitals.

$^{1/2}$H ENDOR Measurements of 1. Strongly−Coupled ^{1}H Derived from H_2. The 35 GHz stochastic field−modulation detected CW ENDOR[32] spectrum of **1** obtained at g_1 shows a ^{1}H doublet centered at the ^{1}H Larmor frequency and split by a hyperfine interaction of $|A(^1H)| = 13.4$ MHz (Figure 2). These peaks are absent

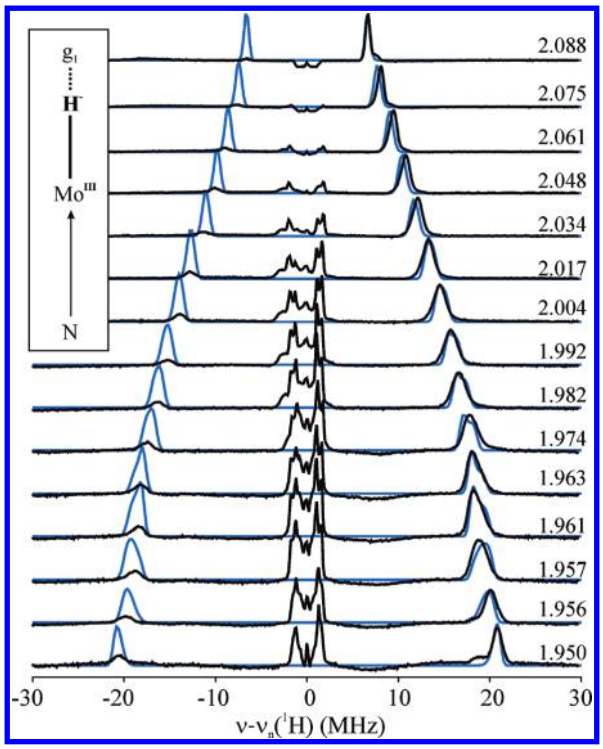

Figure 3. Q-band stochastic 2D field-frequency ew ENDOR pattern for **1** (black) with simulations of the hydride (blue). Conditions: Microwave frequency, 35.305 GHz; modulation amplitude, 0.66 G; temperature, 2 K; rf excitation was broadened to 50 kHz. Simulation parameters: **g** = [2.086, 1.961, 1.947]; **A** = [13, 36, 42.5] MHz, coaxial with **g**; EPR line width, 100 MHz; ENDOR line width, 0.5 MHz. The EPR/ENDOR line widths were deliberately set somewhat smaller than those which best reproduce the measurements to emphasize the absence of splittings in the peaks that occur when **g** and **A** are noncoaxial (see Figure 4 and Supporting Information); this procedure gives rise to the hints of structure near $g \sim 1.97$ and the absence of a shoulder for the simulations at $g_3 = 1.95$ and $g_1 = 2.088$.

in the corresponding ^{1}H spectrum of **Mo**$^2H_2$ (**1(D)**), while Mims 35 GHz ^{2}H pulsed ENDOR spectra of **1(D)** show a corresponding ^{2}H signal. Thus, this ENDOR response is associated with a Mo-bound species that arises from dihydrogen. The ^{2}H ENDOR hyperfine coupling is approximately, but not precisely, related to the ^{1}H ENDOR hyperfine coupling by the ratio of the hydrogen and deuterium nuclear **g** values: $g_n(^1H)/g_n(^2H) = 6.51$. As seen in Figure 2, in which the x axes have been scaled by the ratio of nuclear **g** factors, the ^{2}H ENDOR splitting does not precisely match its ^{1}H counterpart. The difference corresponds to a quite substantial isotope effect on the hyperfine couplings ($A(^1H)/g_n(^1H))/(A(^2H)/g_n(^2H)) = 1.14$), which is caused by differences in Mo−^{1}H/^{2}H zero-point motion that cause differences in spin delocalization.[33]

To determine the hyperfine tensor (**A**) of the Mo-bound hydrogenic species, we collected a full 2D field-frequency pattern comprised of ^{1}H spectra taken at multiple fields across the EPR spectrum (Figure 3). Simulation of this pattern yields excellent agreement with experimental results for a model with a single (type of) ^{1}H whose roughly axial **A** tensor is coaxial with **g**: **A** = $[A_1, A_2, A_3]$ = −[13.0(1), 35.8(3), 42.5(2)] MHz (A_1 parallel to g_1),

(32) Lee, H.-I.; Igarashi, R. Y.; Laryukhin, M.; Doan, P. E.; Dos Santos, P. C.; Dean, D. R.; Seefeldt, L. C.; Hoffman, B. M. *J. Am. Chem. Soc.* **2004**, *126* (31), 9563−9569.

(33) Weber, S.; Kay, C. W. M.; Bacher, A.; Richter, G.; Bittl, R. *ChemPhysChem* **2005**, *6* (2), 292−299.

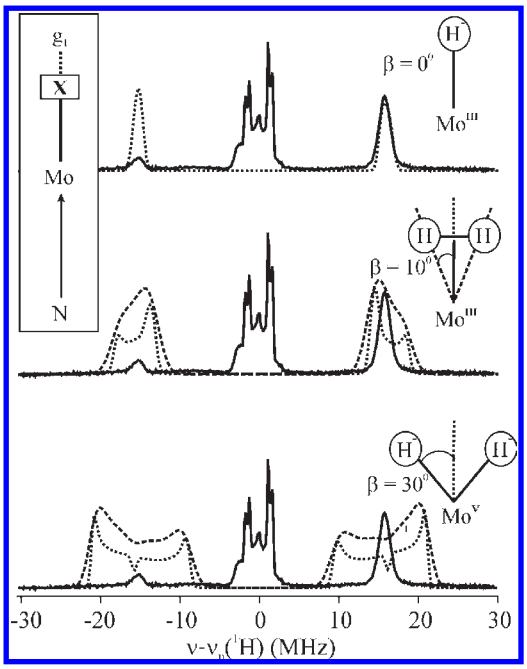

Figure 4. Simulations of ^{1}H ENDOR spectra for models of the reaction product of **Mo**N_2 with H_2, for the spectrum at $g = 1.99$. Simulations are based on the hyperfine tensor determined through the fit to the 2D field frequency plot of Figure 3 (**A** = [13, 36.5, 42] MHz), but with the dipolar interaction rotated by the angle (β) between the hydrogen nuclei and the g_1 axis, taken to lie along the Mo−N_{ax} bond. Top: Mo−H^- bond along g_1, $\beta = 0°$. Middle: Dihydrogen complex; each hydrogen hyperfine tensor is rotated realtive to **g** by $\beta = 10°$. Bottom: Dihydride, $\beta = 30°$. Simulation parameters: **g** = [2.086, 1.961, 1.947], β as indicated. In the second and third cases, two simulations are given, one with small EPR and ENDOR linewidths (150 and 0.5 MHz; dotted lines) to show resolved features, the other with larger EPR and ENDOR linewidths (300 and 2 MHz; dashed lines) to show that these features could not be masked.

corresponding to an isotropic coupling, $a_{iso} = -30.5$ MHz, and an anisotropic (dipolar) interaction, **T** = +[17.5, −5.5, −12] MHz. The relative signs of the components of the **A** and **T** tensors are determined by the simulations.[34]

The absolute signs initially were assigned under the assumption that **T** is dominated by the through-space electron−nuclear dipolar interaction with the Mo(III) electron spin, in which case $T_1 > 0$. This assignment has been confirmed by application of the PESTRE technique, in which the sign of a hyperfine interaction is determined by monitoring the response of the electron−nuclear spin system to multiple Davies sequences at a fixed RF frequency. Figure 5 shows the traces obtained for PESTRE "three-phase" multisequences that separately include RF applied to the ν_+ and ν_- ENDOR peaks of the strongly coupled ^{1}H at g_2. In phase I (no RF), both traces have reached the steady-state electron spin−echo baseline (BSL); in phase II, the RF is applied to a particular branch of the spectrum and converts the spin populations and spin−echo response to their steady-state ENDOR values; in phase III (no RF), the electron−nuclear spin populations give rise to a spin−echo signal denoted as the dynamic reference level (drl), which

(34) The shoulders observed on the ENDOR spectra at g_3 and g_1 can be straightforwardly accounted for in the simulations by increasing the EPR line width. While the simulation does not perfectly reproduce the effect in the data, the differences are acceptable given the approximations used for calculating the EPR line width in the simulation program. Further information and a figure are provided in the Supporting Information.

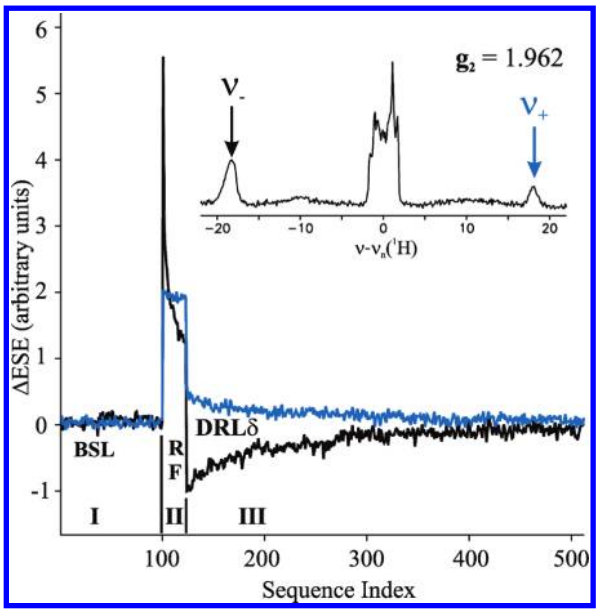

Figure 5. PESTRE spectra measured at the ν_+ (blue) and ν_- (black) peaks of the hydride ENDOR response in **1** at $g_2 = 1.961$. Inset: Davies ^{1}H ENDOR spectrum at g_2. The frequencies at which a PESTRE spectrum was measured are notated by arrows. Conditions, PESTRE: microwave frequency, 34.998 GHz; $\pi = 200$ ns; $\tau = 600$ ns; repetition rate, 40 ms; $t_{rf} = 30\,\mu$s; RF frequency, 72.4 MHz (ν_+) and 36.0 MHz (ν_-). Conditions, ^{1}H ENDOR: $\pi = 200$ ns; $\tau = 600$ ns; repetition rate, 40 ms; $t_{rf} = 30\,\mu$s; RF frequency randomly hopped.

relaxes to the BSL. In these phase III traces, the ν_+ drl relaxes to the BSL from *above*, while the ν_- drl relaxes from *below*. *Either* observation is an unambiguous indication that $A(g_2) < 0$. This verifies the above assignment for the principal values of **A** and **T**, and that $a_{iso} < 0$.[28]

The presence of a large isotropic coupling requires that the exchangeable hydrogenic species is bound to Mo, while $a_{iso} < 0$ indicates that spin is delocalized by spin polarization of the two-electron M−H bond, and not by direct overlap between a partially filled metal-ion orbital and the 1s orbital of H. The assignment of g_1 as lying along the symmetry axis of the parent **Mo**N_2, in conjunction with an ENDOR analysis showing coaxial **A** and **g** tensors for a single type of hydrogenic species, with $T_{max} = T_1$, suggests a model in which heterolytic cleavage of H_2 has yielded a single hydride bound to Mo(III), with a linear N_{ax}−Mo−H^- linkage (Figure 3), σ bonding between the hydrido 1s and Mo d_z^2 orbital, and polarization of this bond by the π electron spin in d_{xz},d_{yz} of Mo. The point-dipole approximation for the anisotropic ^{1}H hyperfine coupling is not highly accurate,[35] but for reference purposes, it would yield a Mo−H bond length of $\lesssim 2$ Å.

To test this model, we compared the experimental 2D ENDOR pattern to those expected for either a dihydrogen complex or a Mo(V)−dihydride complex (Figure 4 and Figures S3 and S4, Supporting Information). These alternate models each would have two magnetically equivalent H atoms, so ENDOR measurements would detect only a single type of hydrogenic species, consistent with experimental results. However, the three models would yield different 2D ENDOR patterns, because each

(35) Snetsinger, P. A.; Chasteen, N. D.; van Willigen, H. *J. Am. Chem. Soc.* **1990**, *112* (22), 8155−8160.

has a distinct value for the angle (β) that the Mo−H vector(s) make with the g_1 (symmetry) axis: for on-axis **Mo**H$^-$, β = 0°; for a dihydrogen complex, reference X-ray structures indicate an expected value of β = 10° for each of the equivalent H atoms;[36] for a dihydride, β = 30−45°.[37,38]

Simulations were generated in which the value of β was increased from 0° to 30°. At all fields away from the high- and low-field edges of the EPR spectrum, as β increases from zero, these spectra show a progressive increase in the breadth of the simulated ENDOR responses and the appearance of new resolved features. Figure 4 presents spectra calculated for a representative field that is sensitive to β (g = 1.99), using the values of β associated with the three structural models, β = 0°, 10°, and 30°. Whereas β = 0° gives an essentially perfect reproduction of the entire 2D pattern, it is clear that, even with β = 10°, the simulations predict that the ENDOR pattern would split into two well-resolved peaks, with the maximum splitting observed at g = 2.017; increasing the line width to merge the peaks would then give an overall feature far broader than observed. Naturally, the problem is exacerbated for β = 30°. Overall, the simulations show that the experimental observations rule out any model for which $\beta \geq 5°$, thus affirming the assignment of **1** as a Mo(III)−H$^-$ center.

Search for ^{2}H$^+$. Heterolytic cleavage of H_2 to generate hydrido-Mo(III) also generates a proton. If this remains bound to **Mo**, it would likely bind to one of the amido nitrogens of the HIPTN$_3$N^{3-} ligand. Simple considerations of geometry indicate that the amido N−H would be ~2.5 Å from the molybdenum and would exhibit a maximum dipolar coupling, $T_{max}(^2H) \sim 1.6$ MHz, and thus should be readily observable. An extensive search was conducted for the signals from such a species using the Mims ^{2}H ENDOR protocol with a wide range of spectroscopic conditions. Under *no* conditions at *any* field within the EPR envelope did the ^{2}H Mims pulsed ENDOR of **Mo**D$_2$ show *any* response that could be reasonably assigned to such a deuteron, as illustrated by the spectrum collected at g_1 (Figure 2) and in the Supporting Information (Figure S4). The absence of an ENDOR response from a weakly coupled deuteron suggests that the proton is transferred to a basic, EPR-silent species during the generation, cooling, and freezing of **Mo**H$_2$, and that species **1** trapped in frozen solution in fact is the [**Mo**(III)H]$^-$ anion.

EPR and ENDOR Studies of Cryoreduced MoH (2). To verify this assignment of **1**, a frozen solution of **Mo**(IV)H (**2**) (d^2; EPR-silent) was radiolytically reduced at 77 K with the goal of directly generating the [**Mo**(III)H]$^-$ anion. Although no crystal structure of **2** is available, its precursor, **Mo**Cl, has been crystallographically characterized.[39] In this structure, the N$_{ax}$−Mo−Cl axis is normal to the plane of the equatorial nitrogens. As complex **2** is synthesized from **Mo**Cl via ligand substitution of the axial chloride with a hydride from the donor species LiBHEt$_3$,[17] the two should share the same structure, with the Cl$^-$ replaced by the H$^-$.

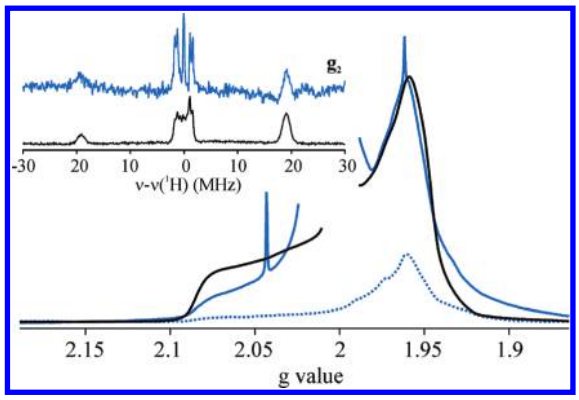

Figure 6. The 35 GHz CW EPR of **1** (black), **2** before cryoreduction, (dashed blue), and **2** after cryoreduction (blue). The cryoreduced **2** shows a 4-fold increase in the reduced species relative to that found in the nonreduced **2**. γ-Irradiation also generates organic radicals whose signal is truncated for clarity, as well as hydrogen atoms within the quartz tubes, which contribute the characteristic sharp hyperfine doublet with $|A(^1H)|$ = 507 G. Inset: 35 GHz ^{1}H stochastic field-modulated ENDOR spectra of cryoreduced **2** (blue) and **1** (black) measured at g_2 = 1.947. Conditions, EPR of **2**: microwave frequency, 35.289 GHz; microwave power, 0.1 mW; modulation amplitude, 0.33 G; time constant, 64 ms; scan time, 2 min; receiver gain divided out of the spectra of **2**; intensity of **1** arbitrarily adjusted to match intensity at g_2 of **2**. Conditions, ENDOR: microwave frequency, 35.231 GHz; modulation amplitude, 0.67 G; temperature, 2 K; stochastic sequence (delay/sample/RF), 0.75/1.25/0.5 ms; rf excitation was broadened to 50 kHz.

Figure 6 shows overlaid EPR spectra of **1** and of **2**, both before and after cryoreduction. Untreated **2** shows a weak EPR signal that is nearly identical to that of **1**. Upon cryoreduction, this signal increases approximately 5-fold, indicating that this signal is associated with the [**Mo**H]$^-$ anion; its **g** values of [2.086, 1.961, 1.949] are the same as those of **1**. A comparison of the ^{1}H 2D ENDOR patterns of cryoreduced **2** and of **1**, as illustrated by the ^{1}H ENDOR spectra at g_2 (Figure 6, inset), shows that the two species give identical spectra at all fields. These EPR and ENDOR experiments thus establish that **1** indeed is the [**Mo**(III)H]$^-$ anion.

^{14}N ENDOR Measurements of 1. Figure 7 presents ^{14}N Davies pulsed ENDOR spectra of **1** collected at the low-field (g_1 = 2.086) and high-field (g_3 = 1.947) edges of its EPR envelope. These two spectra reveal features from two distinct types of nitrogen signals: sharp, well-defined signals that are assigned to the axial amino nitrogen (N$_{ax}$) and broader signals that are attributed to the combined ENDOR response of the three "equatorial" amido nitrogens (N$_{eq}$) of the HIPTN$_3$N^{3-} ligand. The patterns for the two types of ^{14}N overlap across the entire EPR envelope, but because the features from the axial nitrogen are significantly sharper, the two signals are easily distinguished at all fields. In addition, the spectra clearly show $\Delta m_I = \pm 2$ "double quantum" transitions[24] for both the ν_+ and ν_- manifolds of ^{14}N$_{ax}$ across the entire EPR envelope (Figure S6, Supporting Information), giving an experimentally independent check of our assignments. We note that the ^{14}N spectra of the [**Mo**H]$^-$ anions of cryoreduced **2** and **1** are identical (Figure S5, Supporting Information), as required.

(36) Kubas, G. J.; Burns, C. J.; Eckert, J.; Johnson, S. W.; Larson, A. C.; Vergamini, P. J.; Unkefer, C. J.; Khalsa, G. R. K.; Jackson, S. A.; Eisenstein, O. *J. Am. Chem. Soc.* **1993**, *115* (2), 569−81.
(37) Shin, J. H.; Churchill, D. G.; Bridgewater, B. M.; Pang, K.; Parkin, G. *Inorg. Chim. Acta* **2006**, *359* (9), 2942−2955.
(38) Martins, L. M. D. R. S.; Alegria, E. C. B. A.; Hughes, D. L.; Frausto da Silva, J. J. R.; Pombeiro, A. J. L. *Dalton Trans.* **2003** (*19*), 3743−3750.
(39) Ritleng, V.; Yandulov, D. V.; Weare, W. W.; Schrock, R. R.; Hock, A. S.; Davis, W. M. *J. Am. Chem. Soc.* **2004**, *126* (19), 6150−6163.

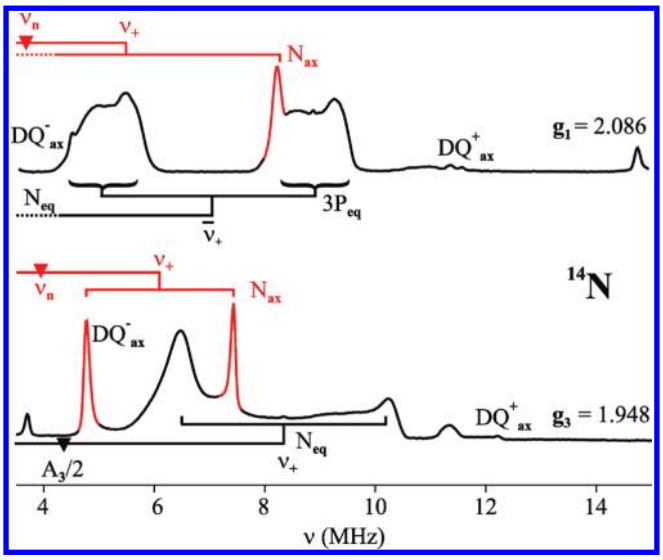

Figure 7. Davies ^{14}N pulse ENDOR of **1** at $g_1 = 2.086$ and $g_3 = 1.947$. The axial nitrogen (N_{ax}) and equatorial nitrogen (N_{eq}) quadrupole split peaks for the ν_+ manifold are labeled. The "double quantum" ($\Delta m_I = \pm 2$) transitions for both the α and β electron manifolds are labeled. Conditions: microwave frequency, 34.998 GHz; $\pi = 200$ ns; $\tau = 1000$ ns; $t_{rf} = 30$ μs; repetition rate, 20 ms; RF frequency randomly hopped.

Axial Nitrogen (N_{ax}). In Figure 7, the $^{14}N_{ax}$ nucleus contributes a sharp, quadrupole-split, ν_+ doublet at both g_3 and g_1, with $A(g_3) = 4$ MHz and $|3P(g_3)| = 2.7$ MHz (bottom) and with $A(g_1) = 4$ MHz and $|3P(g_1)| = 5.5$ MHz (top). For the 2D field-frequency pattern of N_{ax} (Figure 8 and Figure S6, Supporting Information), the ENDOR spectra taken across the EPR envelope are reproduced by simulations that employ an essentially isotropic hyperfine tensor ($a_{iso} = 4$ MHz) and an axial quadrupole tensor ($\mathbf{P} = [P_1, P_2, P_3] = [-1.82, 0.91, 0.91]$ MHz). The relative signs of the P_i ($i = 1-3$) are fixed by the simulations; the absolute signs are established as discussed by Lucken.[40] **P** is coaxial with **g**, with the unique value, P_1, lying along g_1. The form of **P** is precisely as expected for the coordinated trialkyl amino N_{ax} nitrogen,[40] for which the unique quadrupole direction (P_1) must lie along the Mo−N_{ax} bond (g_1), as observed. These measurements thus directly confirm the structural model of a linear N_{ax}−Mo−H^- axis (Figure 3, inset), with the unique axes of **g**, **P** for N_{ax}, and **A** for the hydride all lying along this molecular axis.

Equatorial Nitrogens (N_{eq}). In the ^{14}N ENDOR spectrum at g_1 (Figure 7, top), the three $^{14}N_{eq}$ nuclei combine to give a single quadrupole-split ν_+ doublet. Unlike the extremely sharp N_{ax} signal (fwhm = 0.5 MHz), the individual $\nu_{+,\pm}$ features for $^{14}N_{eq}$ at g_1 are far broader (fwhm = 1.1 MHz). If the anion had precise C_3 symmetry with g_1 as the symmetry axis, the three equatorial nitrogen ligands would be magnetically equivalent when viewed with the field along g_1, and the ν_+ doublet would likely be sharp, as it is for N_{ax}. That this is not the case suggests that the anion is statically distorted from trigonal symmetry, that the hyperfine and quadrupole couplings differ for the three ^{14}N's, and that the $^{14}N_{eq}$ ENDOR spectrum at g_1 reflects a range of values for one or both of these

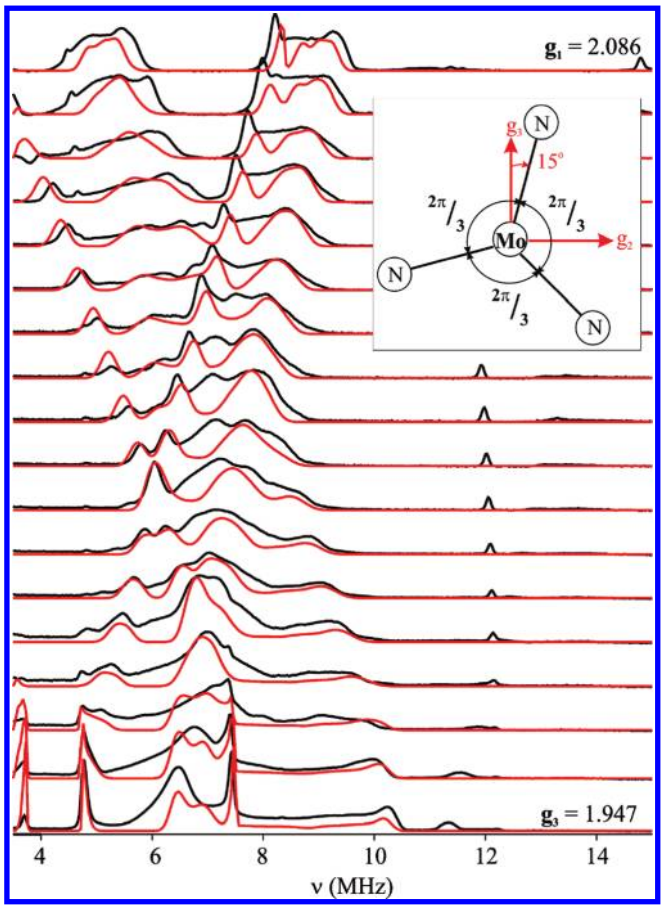

Figure 8. Davies ^{14}N pulse ENDOR of **1**, 2D field-frequency pattern with simulations. The simulation pattern is the sum of the simulations for the axial nitrogen and three sets of three simulations for the equatorial nitrogens. Inset: The rotation angle α is defined as a rotation around the g_1 axis (normal to the plane of the equatorial nitrogens). The angles utilized for the three equatorial nitrogens are indicated in the diagram. Simulation parameters: microwave frequency, 34.998 GHz; **g** = [2.086, 1.961, 1.947]; EPR line width, 150 MHz; $g_1 = z$. Axial N: **A** = [3.95, 4, 4.05] MHz; **P** = [−1.82, 0.91, 0.91] MHz; ENDOR line width, 0.01 MHz; **g**, **A**, and **P** are coaxial; allowed transitions included. Equatorial N: **A** = [{5.39, 6.25, 7.11}, 5.8, 8.7] MHz; **P** = [−1.33, 0.03, 1.3] MHz; ($\alpha\beta\gamma$) = ({15, 135, 75}, 0, 0); ENDOR line width, 0.25 MHz, only plus manifold included.

parameters. If we consider the two extremes, well-defined hyperfine coupling at g_1 but distributed quadrupole couplings, or vice versa, in the first case the breadth of the $\nu_{+,\pm}$ features would correspond to a hyperfine coupling of $A(g_1) = 6.6$ MHz and a quadrupole splitting range of $2.7 \leq |3P(g_1)| \leq 4.5$ MHz, while in the second the breadth would imply a hyperfine range of $5.4 \leq A(g_1) \leq 7.1$ MHz, with a quadrupole splitting of $|3P(g_1)| = 3.9$ MHz.

In the spectrum collected at g_3 (Figure 7, bottom), the three $^{14}N_{eq}$'s combine to give an ENDOR pattern with features that are narrower than at g_1, with $A(g_3) \sim 8.8$ MHz and $|3P(g_3)| \sim 3.8$ MHz, but again, the N_{eq} features are broader than those of the corresponding N_{ax} doublet. However, in this case, the magnetic field lies in the equatorial plane, and of necessity the angle between the field and the Mo−N_{eq} bond is not the same for all three N_{eq}'s. As such, in spectra collected at g_3, the three nuclei could not have the same hyperfine and quadrupole couplings, even if they were physically and chemically equivalent.

(40) Lucken, E. A. C. *Nuclear Quadrupole Coupling Constants;* Academic Press: New York, 1969; p 360.

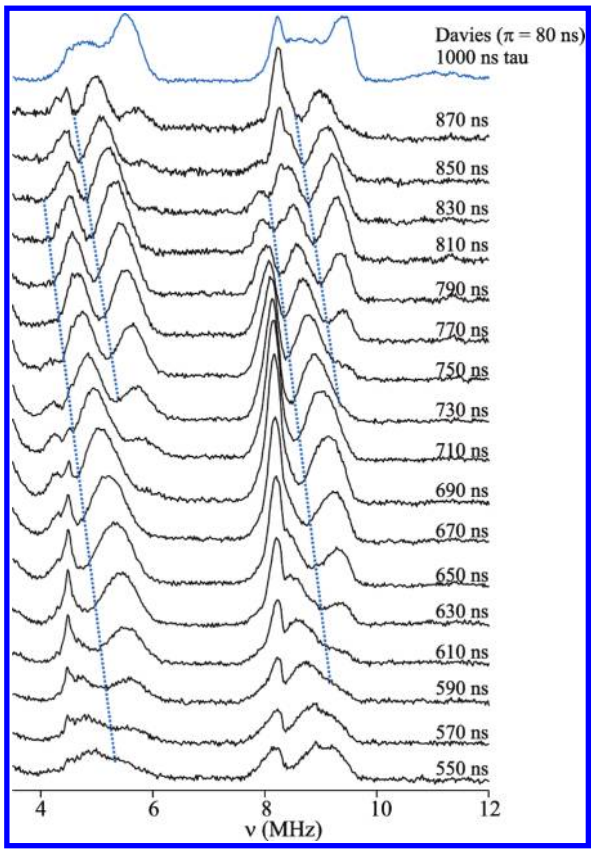

Figure 9. Mims ^{14}N pulse ENDOR of **1** at $g_1 = 2.086$. The value of τ is varied from 550 to 870 ns to observe the effect of hyperfine suppression on the ^{14}N ν_+ ENDOR pattern. Due to the quadrupole splitting inherent to the ^{14}N pattern, an observation of suppression occurs for a given hyperfine coupling at the frequencies $A \pm {}^3/_2P$ MHz. This splitting is delineated by the separation between the dashed blue lines. Conditions: microwave frequency, 35.017 GHz; repetition time, 20 ms; $\pi/2 = 50$ ms; $\tau = 550-870$ ns; $t_{rf} = 30\ \mu$s; RF frequency randomly hopped.

To determine the origin of the breadth of the $^{14}N_{eq}$ $\nu_{+,\pm}$ feature at g_1, we used the hyperfine suppression effect inherent to the Mims ENDOR technique. For a Mims sequence with pulse interval, τ, the ν_+ ENDOR doublet would be suppressed for nuclei with $A_1(^{14}N_{eq}) = n/\tau$ ($n = 0, 1, 2, ...$) regardless of the value of $3P_1$. If suppression is observed for a range of τ values, this would imply a corresponding spread in $A_1(^{14}N_{eq})$, while the breadth of a suppression hole would be determined by the spread in values of the quadrupole splitting, $3P_1$.

Figure 9 shows a 2D τ-frequency plot of Mims ENDOR spectra collected at g_1 over the range $550 \le \tau \le 870$ ns. Both branches of the $\nu_{+,\pm}$ doublet show sharp suppression holes over the range of pulse intervals, τ. The sharp suppression holes indicate that the quadrupole splitting, $3P_1$, is well-defined, while suppression over a range in τ indicates that the $^{14}N_{eq}$'s exhibit a corresponding range in $A(g_1)$. Thus, the second limiting case noted above applies: $5.4 \le A(g_1) \le 7.1$ MHz, with $|3P(g_1)| = 3.9$ MHz. A reasonable simulation of the $^{14}N_{eq}$ g_1 ENDOR spectrum based on such a hyperfine distribution is obtained by modeling it with the summation of ENDOR simulations generated with three equally probable A_1 hyperfine couplings, $A_1 = \{5.39, 6.25, 7.11\}$ MHz, each with $|P_1| = 1.33$ MHz (Figure 8, top).

The next step in characterizing the $Mo-N_{eq}$ bonding was determination of the full $^{14}N_{eq}$ hyperfine and quadrupole tensors for the three $^{14}N_{eq}$'s from a 2D field/frequency pattern of ^{14}N spectra collected across the EPR envelope (Figure 8). For simplicity in analysis, we took the $Mo-N_{eq}$ bonds to be orthogonal to g_1 and trigonally arranged ($N_{eq}-Mo-N_{eq} = 120°$ for adjacent N_{eq}), each with coaxial **A** and **P** tensors whose (A_1, P_1) principal axes lie parallel to g_1, and with the (A_3, P_3) principal axis for the three N making angles, α, $\alpha + 2\pi/3$, $\alpha + 4\pi/3$, with g_3. If we imagine (A_3, P_3) to lie along the $Mo-N_{eq}$ bond, then α would represent the rotation of the N_{eq} equilateral triangle, relative to the g_3 principal axis, with $\alpha = 0$ placing the $Mo-N_{eq}$ bond of one nitrogen along g_3 (Figure 8, inset). We note, however, that the model does not require that A_3 and P_3 be coincident with $Mo-N_{eq}$, only that they have the same orientation relative to $Mo-N_{eq}$ for all three equatorial nitrogens. The angle α turns out to be particularly important in reproducing the ENDOR spectra at fields in the vicinity of g_2 and g_3. The simplest model that effectively reproduces the pattern assigns to each of the N_{eq}'s an equal probability that it has each of the three values of $A_1 = \{5.39, 6.25, 7.11\}$ MHz determined in the above analysis of the g_1 spectrum, as well as $|P_1| = 1.33$ MHz. All of the other tensor components were assumed to be the same for the three N_{eq}'s. This model was implemented by summing the corresponding nine simulations at each g value.

The outcome of numerous simulation attempts was that the 2D pattern can be well simulated (Figure 8) by combining the nine sets of simulations for interaction tensors with components $\mathbf{A} = [\{5.39, 6.25, 7.11\}, 5.8, 8.7]$ MHz and $\mathbf{P} = [-1.33, 0.03, 1.3]$ MHz, and with the N_{eq} triangle rotated relative to g_3 by the angle $\alpha = 15°$. Considering the limited resolution in the ENDOR spectra, and the need to sum multiple spectra from inequivalent ^{14}N, the use of more complex structural models, for example placing Mo out of the N_{eq} plane, or allowing for angular distortions within the N_{eq} plane, is unwarranted. Nonetheless, this range in coupling parameters for the N_{eq} nuclei is direct evidence for a static JT distortion of the **Mo** equatorial plane.

Discussion

We have carried out a comprehensive EPR and ENDOR study of the product of reaction between $[HIPTN_3N]MoN_2$ and H_2. Analysis of ^1H ENDOR spectra taken at multiple fields across the EPR envelope (2 K) shows that the principal species in frozen solution is the $[\mathbf{Mo}H]^-$ anion, **1** (Scheme 1). This anion is assigned as having a Mo(III), $[d_{xz}, d_{yz}]^3$ orbital configuration, as proposed for the parent $\mathbf{Mo}N_2$ complex, and therefore is susceptible to a Jahn–Teller (JT) distortion. We first discuss the properties and structure of the $[\mathbf{Mo}H]^-$ anion as determined by $^{1,2}H$ and ^{14}N ENDOR. We next discuss JT effects in the anion in light of the structural results and the **g** tensor of this anion. Lastly, we compare this study of **1** trapped in frozen solution with the recent study of the reaction of $[HIPTN_3N]MoN_2$ and H_2 in fluid solution.

$[\mathbf{Mo}H]^-$ (1) in Frozen Solution. $^{1,2}H$ ENDOR measurements of **1** reveal the presence of a single hydride bound to Mo, the result of heterolytic cleavage of H_2. In combination with ^{14}N ENDOR measurements of the axial amino

nitrogen of the [HIPTN$_3$N]Mo center, these observations reveal the presence of a structural axis that passes through the hydride, the Mo, and the axial amino nitrogen of the [HIPTN$_3$N]$^{3-}$ ligand, and that this axis is coincident with the unique magnetic axis (g_1) of the molecule. These conclusions are confirmed by EPR and ENDOR measurements (^{1}H and ^{14}N) which show that **1** trapped in frozen solution is essentially identical to the anion formed when **Mo**(IV)H (**2**) is radiolytically reduced to the [**Mo**(III)H]$^-$ anion at 77 K.

^{14}N ENDOR measurements also characterized the three nitrogens of [HIPTN$_3$N]$^{3-}$ that form an equatorial plane perpendicular, or nearly so, to the [H$^-$−Mo−N$_{ax}$] axis. These revealed that the three nitrogens are magnetically similar, as would be expected for a system possessing a pseudo-C_3 axis of symmetry, but that they are not equivalent, as would be the case for a trigonally symmetric molecule or one undergoing a dynamic JT distortion. Thus, they indicate that the hydride anion instead exhibits a static JT distortion.

Where is the Proton? The assignment of **1** as a Mo-hydride anion generated by heterolytic cleavage of H_2 raises the question: where is the partner proton generated in parallel? Our initial expectation was that the proton would bind to one of the three basic amido nitrogens of the [HIPTN$_3$N]$^{3-}$ ligand. However, extensive efforts failed to disclose either a ^{1}H or ^{2}H ENDOR signal from this proton, whereas such a proton is readily detected when [**Mo**]CO is treated with acid (unpublished). Moreover, preliminary DFT computations[41] confirm that such a protonation would decrease the N$_{ax}$−Mo−H$^-$ angle from 180°, such that either the Mo−N$_{ax}$ or Mo−H$^-$ bonds, and thus either the $^{1/2}$H *or* the ^{14}N$_{ax}$ hyperfine (and ^{14}N$_{ax}$ quadrupole) tensors, could be coaxial with **g**, but not both, contrary to observation.

If the proton formed by H_2 heterolysis does *not* reside on an equatorial nitrogen of the hydrido complex **1**, what, then, is its fate? In the solution study, it was proposed that the heterolytically cleaved species (denoted **Mo**HN$_H$), itself in equilibrium with "**Mo**H$_2$", further is in equilibrium with an arm-off form, and that this is unstable to decomposition and ligand loss.[14] We suggest that, during the process of freezing a sample of "**Mo**H$_2$", free ligand, produced by decomposition of either the **Mo**HN$_H$ or the "arm-off" species, or other EPR-silent products of decomposition, accept the proton from **Mo**HN$_H$, thereby generating the hydride anion **1**, and that this process pulls the equilibrium involving "**Mo**H$_2$" completely to **1**.

The Jahn−Teller Effect and the g and Hyperfine Tensors of 1. The hydrido-Mo(III) anion revealed by ENDOR spectroscopy would have **g** values of $g_{||} = 4$ and $g_\perp = 0$ in its idealized C_3 geometry. Thus, the discussion of the **g** tensor must be carried out in a different framework than would be the case if it had been found to be either a lower-symmetry H_2 or a dihydrido complex. The decrease in $g_{||}$ to $g_1 = 2.086$ and the increases in $g_\perp$ to $g_{2,3} \sim 2$ is most informatively discussed in terms of the reduction in symmetry from C_3 as would occur with a PJT distortion, as described by eq 1 and 2, with $r \sim 20$. The small rhombicity of the **g** tensor, attributable to the influence of second-order contributions to **g** from other d orbitals, should be more pronounced in **1** than in **Mo**N$_2$ because the absence of a strong π-backbonding axial ligand in **1** should diminish the energy difference between the d$(xz,yz)^3$ orbitals and the higher-lying empty d(z^2) orbital, increasing the second-order contributions; furthermore, the narrow EPR lines of **1** improve the ability to observe this splitting. This picture is supported by the observation that, unlike **Mo**N$_2$, the EPR spectrum of **1** broadens with increasing temperature, indicating that **1** has lower-lying excited states than **Mo**N$_2$.[42] The analysis of the ^{14}N ENDOR signals from the in-plane ^{14}N$_{eq}$ shows that **1** undergoes a localized, not a dynamic, PJT distortion. Localization can be caused by quadratic terms in the vibronic interaction,[43] or by environmental trapping of the distorted configuration(s).

Thus, the complete set of magnetic properties of **1** can be interpreted in terms of a hydrido-Mo(III) anion undergoing a PJT distortion. However, the large value for the linear JT parameter, r (eq 1), for **1** implied by this analysis, compared to that for **Mo**N$_2$, is surprising. The obvious explanation for why r for anionic **1** is so large is that **1** experiences a large environmental energy, V_E. However, this does not appear to represent a "solvent effect", because, unlike **Mo**N$_2$, there is a negligible effect on the EPR spectrum of **1** with solvent variation. Also, it does not seem plausible that the larger value of r simply reflects a larger value of the linear JT term, V_{JT}, in the numerator of r (eq 1). This parameter depends on the linear vibronic coupling parameter (F) and the force constant (K) for the composite JT-active vibration, through the relationship, $V_{JT} \propto F^2/K$. The composite vibration likely is associated with **Mo** bonds to the [HIPTN$_3$N]$^{3-}$ ligand, which are the same for both systems; to the extent that K is associated with the axial ligand, the force constants for Mo−H and Mo−N are expected to differ very little.[17,44,45]

One possible explanation is that anionic **1** forms a tight ion pair with an unidentified counterion, and that $V_\delta \sim V_E$, an electrostatic interaction potential between the ions. However, the absence of any significant changes in the **g** values for **1** when other cations (salts) were added to the solution, plus the observation of an identical **g** tensor for **1** formed by cryoreduction of **Mo**(IV)H (**2**) in frozen solution, where a tight ion pair cannot form, makes this proposal unlikely. Instead, we surmise that the inferred decrease in the energy gap between the partially filled d[xz, yz] and the empty d[xy, x^2-y^2] in **1**, as compared to **Mo**N$_2$, allows mixing of these orbitals, leading to a

(41) Density Functional Theory (DFT) calculations were performed with the Amsterdam Density Functional (ADF) software package (ADF version 2007.01, SCM, Theoretical Chemistry, Vrije Universiteit, Amsterdam, The Netherlands, http://www.scm.com, accessed Dec 2009) with a BLYP functional in the spin-unrestricted formalism. Geometry optimization calculations on [**Mo**H]$^-$ and **Mo**HN$_H$ used a TZ2P basis set with a small core potential for all atoms. For calculation of all hyperfine, quadrupole, and **g**-tensor values, no core potential was used. All calculations used a reduced structure for Mo in which the HIPT groups were replaced with phenyls.

(42) Abragam, A.; Bleaney, B. *Electron Paramagnetic Resonance of Transition Ions*; Dover Publications, Inc.: New York, 1986.

(43) Bersuker, I. B., *The Jahn-Teller Effect*, 1st ed.; Cambridge University Press: New York, 2006; pp 54−62.

(44) Force constants (K) for **Mo**-H and **Mo**-N were calculated using IR stretching frequencies of 1748 and 453 cm^{-1}, respectively, yielding K(**Mo**-H) = 160 N m^{-1} (Yandulov et. al) and K(**Mo**-N) = 148 N m^{-1} (Stephan et. al).

(45) Stephan, G. C.; Peters, G.; Lehnert, N.; Habeck, C. M.; Naether, C.; Tuczek, F. *Can. J. Chem.* **2005**, *83* (4), 385−402.

distortion that in effect amounts to an additional PJTE.[46] DFT computations to test this idea, as well as to give deeper insights into the bonding and hyperfine interactions in this unusual $S = 1/2$ complex, will be reported in due course.

Summary. An EPR and $^{1/2}H/^{14}N$ ENDOR study of the product of the reaction between **Mo**N_2 and H_2 (**1**) that is trapped in frozen solution, including the determination of hyperfine signs through the newly developed PESTRE technique, has shown **1** to be the [**Mo**(III)H]$^-$ anion that forms as a result of heterolytic cleavage of H_2. The measurements show that **1** contains a linear $N_{eq}-Mo-H^-$ axis along which lies the "unique" axis of the **g** tensor for the complex. Determination of the hyperfine and quadrupole interaction tensors for the three equatorial nitrogens shows that they have similar properties, but that the complex shows a small, static distortion from an idealized trigonal geometry. This distortion is discussed in terms of the PJTE expected for low-spin Mo(III) in a trigonal environment. The generation of this species is discussed in terms of the equilibria between the "**Mo**H_2", **Mo**HN_H, and a previously postulated "arm-off" species and supports the conclusion that the "**Mo**H_2" complex is in dynamic equilibrium between these several forms. Beyond this, the finding of a nearly axial hyperfine coupling tensor for a hydride bound to molybdenum supports the proposal that hydrogenic species with rhombic hyperfine tensors bound to the FeMo-cofactor of the nitrogense E_4 intermediate are hydrides that bridge two metal ions, rather than terminal hydrides.[16]

(46) Bersuker, I. B., *The Jahn-Teller Effect*; 1st ed.; Cambridge University Press: Cambridge, U. K., 2006; pp 353−478.

Acknowledgment. R.A.K. and B.M.H. thank Dr. Rebecca McNaughton and Dr. Peter Doan for helpful discussions, and Clark Davoust for his technical support. We thank Dr. Roman Davydov for carrying out cryoreductions. We thank Prof. Howard Halpern (University of Chicago) for providing access to the Gammacell irradiator. This work has been supported by the NIH (GM 31978, RRS; HL 13531, BMH) and the NSF (MCB0723330, BMH). D.G.H.H. thanks The Netherlands Organization for Scientific Research (NWO−CW) for a postdoctoral fellowship

Supporting Information Available: Six figures (Figure S1−S6). This material is available free of charge via the Internet at http://pubs.acs.org.